Global simulations of electromagnetic turbulence in stellarators using EUTERPE in stellarator plasmas

A. Mishchenko[1*], M. Borchardt[1], R. Hatzky[2], R. Kleiber[1], A. Könies[1], Y. Narbutt[1], C. Nührenberg[1], E. Sanchez[3], P. Xanthopoulos[1], G. Roberg-Clark[1], and G. Plunk[1]

[1]Stellarator Theory, Max Planck Institute for Plasma Physics, Germany

[2] Numerical Methods in Plasma Physics, Max Planck Institute for Plasma Physics, Germany

[3] CIEMAT Madrid, Spain

EUROfusion's TSVV Tasks 10, 12, 13

This work has been carried out within the framework of the EUROfusion Consortium and has received funding from the Euratom research and training programme 2014-2018 under grant agreement No 633053. The views and opinions expressed herein do not necessarily reflect those of the European Commission.

Motivation

- Most of stellarator turbulence studies are in a flux tube
- But: flux-tube modeling is more questionable in stellarators than it is in tokamaks
  - Flux tubes are not equivalent (in contrast to tokamaks): stellarators are intrinsically poloidally-global
  - Generally, radial bounce-averaged drifts do no vanish (in contrast to tokamaks): stellarators are intrinsically radially-global
  - No good way to incorporate ambient E_r in a flux tube

Status: only a handfull of global turbulence simulations (EUTERPE, GENE-3D, XGC-S, GTC) are available for stellarators; mostly electrostatic

Challenge: global electromagnetic turbulence in stellarator (W7-X) geometry

KBM growth rate non-zonal transition in EM regime

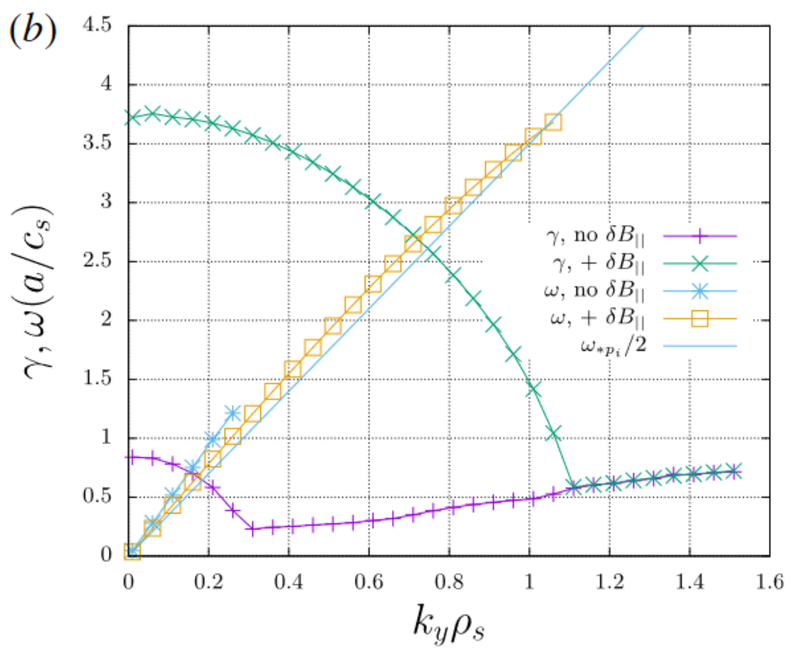

spectra for W7-X from GENE simulations. (*a*) $a/L_{Ti,e} = 3$. (*b*) $a/L_{Ti,e} = 7$.

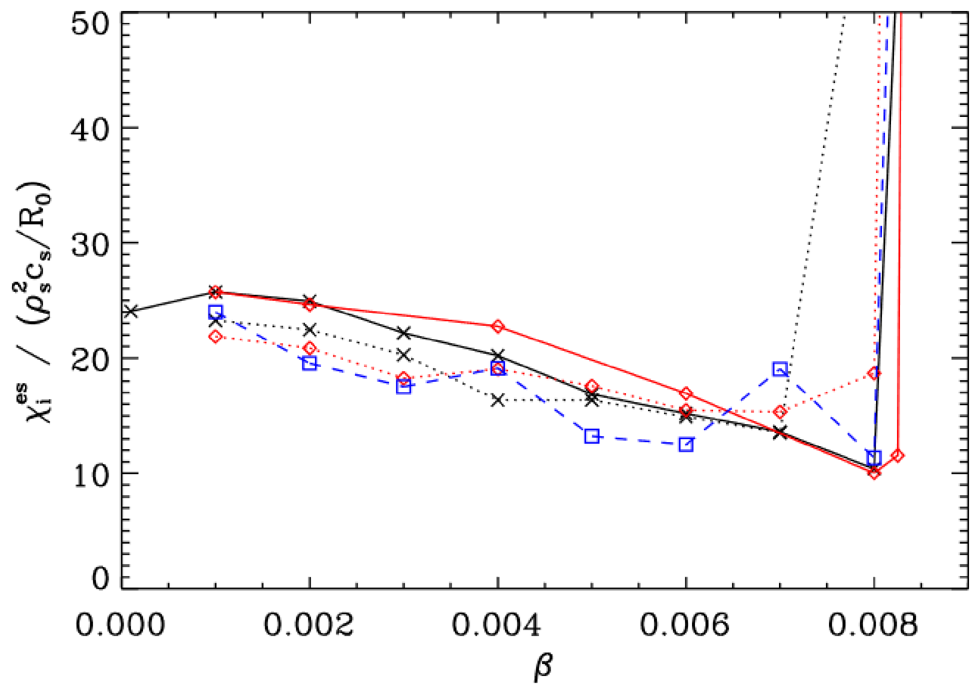

FIG. 1. Results from gyrokinetic codes GENE (black crosses), GYRO (red diamonds), and GKW (blue squares) for $\beta \leq \beta_{crit}^{NZT}$: plotted is the ion electrostatic heat diffusivity. The near-vertical lines at the threshold illustrate a transition to very large transport values; for all β scans shown, this occurs above $\beta = 0.8\%$ but below $\beta = 0.85\%$. Good quantitative agreement is found both for the pre-NZT transport and the NZT threshold. Dotted lines (GENE and GYRO) indicate sensitivity tests with slightly different numerical settings.

K. Aleynikova, JPP 2018

M. Pueschel, PoP 2013

KBMs have finite γ for $k_y\,\rho_s \to 0$

Ion heat flux $\chi_i \to \infty$ at finite β

Global approach can resolve problems

Electromagnetic turbulence in tokamak plasmas

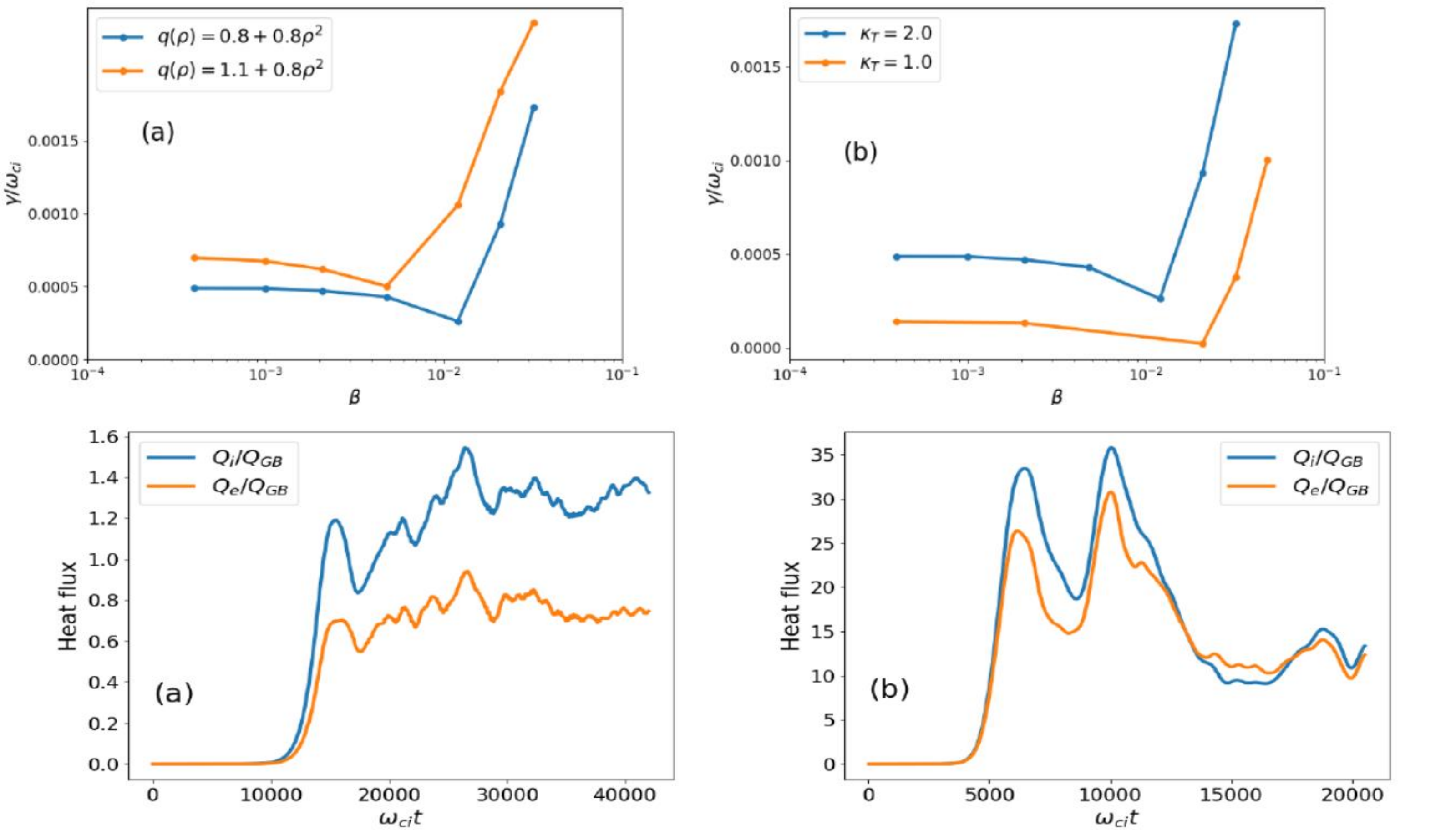

(1) Linear growth rate in circular-shaped tokamak for different safety factor profiles and temperature gradients showing electromagnetic ITG-to-KBM transition (ORB5 simulations on Marconi100, CINECA). Heat flux in the gyro-Bohm units for (a) β = 0.1% (electromagnetic ITG) and (b) β = 2.08% (KBM regime). The heat flux is considerably larger in KBM regime.

No “electromagnetic run-away” in global tokamak simulations.

Gyrokinetic equations (mixed variables)

The equations include the gyrokinetic Vlasov equation:

https://doi.org/10.1088/1361-6587/ac0bcb

$$\frac{\partial f_{1s}}{\partial t} + \dot{\boldsymbol{R}} \cdot \frac{\partial f_{1s}}{\partial \boldsymbol{R}} + \dot{v}_\parallel \frac{\partial f_{1s}}{\partial v_\parallel} = -\dot{\boldsymbol{R}}^{(1)} \cdot \frac{\partial F_{0s}}{\partial \boldsymbol{R}} - \dot{v}_\parallel^{(1)} \frac{\partial F_{0s}}{\partial v_\parallel} , \quad (1)$$

the equations for the gyro-center orbits:

$$\dot{\boldsymbol{R}} = \dot{\boldsymbol{R}}^{(0)} + \dot{\boldsymbol{R}}^{(1)} , \quad \dot{v}_\parallel = \dot{v}_\parallel^{(0)} + \dot{v}_\parallel^{(1)} \quad (2)$$

$$\dot{\boldsymbol{R}}^{(0)} = v_\parallel \boldsymbol{b}_0^* + \frac{1}{qB_\parallel^*} \boldsymbol{b} \times \mu \nabla B , \quad \dot{v}_\parallel^{(0)} = -\frac{\mu}{m} \boldsymbol{b}_0^* \cdot \nabla B \quad (3)$$

$$\dot{\boldsymbol{R}}^{(1)} = \frac{\boldsymbol{b}}{B_\parallel^*} \times \nabla \left\langle \phi - v_\parallel A_\parallel^{(\mathrm{s})} - v_\parallel A_\parallel^{(\mathrm{h})} \right\rangle - \frac{q}{m} \langle A_\parallel^{(\mathrm{h})} \rangle \boldsymbol{b}_0^* \quad (4)$$

$$\dot{v}_\parallel^{(1)} = -\frac{q}{m} \left[\boldsymbol{b}^* \cdot \nabla \left\langle \phi - v_\parallel A_\parallel^{(\mathrm{h})} \right\rangle + \frac{\partial}{\partial t} \left\langle A_\parallel^{(\mathrm{s})} \right\rangle \right] - \frac{\mu}{m} \frac{\boldsymbol{b} \times \nabla B}{B_\parallel^*} \cdot \nabla \left\langle A_\parallel^{(\mathrm{s})} \right\rangle \quad (5)$$

$$\boldsymbol{b}^* = \boldsymbol{b}_0^* + \frac{\nabla \langle A_\parallel^{(\mathrm{s})} \rangle \times \boldsymbol{b}}{B_\parallel^*} , \quad \boldsymbol{b}_0^* = \boldsymbol{b} + \frac{m v_\parallel}{q B_\parallel^*} \nabla \times \boldsymbol{b} \quad (6)$$

$$B_\parallel^* = B + \frac{m v_\parallel}{q} \boldsymbol{b} \cdot \nabla \times \boldsymbol{b} , \quad (7)$$

Field equations:

$$-\nabla \cdot \left(\frac{n_0}{B \omega_{ci}} \nabla_\perp \phi \right) = \bar{n}_{1i} - \bar{n}_{1e}$$

$$\frac{\partial}{\partial t} A_\parallel^{(\mathrm{s})} + \boldsymbol{b} \cdot \nabla \phi = 0 ,$$

$$\sum_{s=i,e} \frac{\beta_s}{\rho_s^2} A_\parallel^{(\mathrm{h})} - \nabla_\perp^2 A_\parallel^{(\mathrm{h})} = \mu_0 \sum_{s=i,e} \bar{j}_{\parallel 1s} + \nabla_\perp^2 A_\parallel^{(\mathrm{s})}$$

Gyrokinetic particle-in-cell codes: EUTERPE

- "Klimontovich" representation for perturbed distribution function:

$$\delta f_s(\boldsymbol{R}, v_\|, \mu, t) = \sum_{\nu=1}^{N_p} w_{s\nu}(t)\delta(\boldsymbol{R} - \boldsymbol{R}_\nu)\delta(v_\| - v_{\nu\|})\delta(\mu - \mu_\nu) \ ,$$

- Maxwellian distribution for all species:

$$F_{0s} = n_0 \left(\frac{m}{2\pi T_s} \right)^{3/2} \exp\left[- \frac{m_s v_\|^2}{2T_s} \right] \exp\left[- \frac{m_s v_\perp^2}{2T_s} \right]$$

- Finite-element discretization for fields:

$$\phi(\boldsymbol{x}) = \sum_{l=1}^{N_s} \phi_l(t)\Lambda_l(\boldsymbol{x}) \ , \quad A_\|(\boldsymbol{x}) = \sum_{l=1}^{N_s} a_l(t)\Lambda_l(\boldsymbol{x}) \ ,$$

- 1995: GYGLES is developed at SPC (CRPP) with adiabatic electrons
- 1999: ORB5 and EUTERPE are developed at SPC (CRPP)
- 2001: kinetic electrons implemented in GYGLES at IPP
- 2004: EUTERPE employed for W7-X; GYGLES becomes electromagnetic (IPP)
- 2008: ORB5 becomes electromagnetic (joint development IPP/SPC/UW)
- 2009: EUTERPE becomes electromagnetic (IPP)
- 2014-2019: EUTERPE, GYGLES and ORB5 implement mixed variables
- Collaboration today: SPC, IPP, Ciemat, ENEA, UniWarwick, IPR

Down-scaled W7-X (KJM)

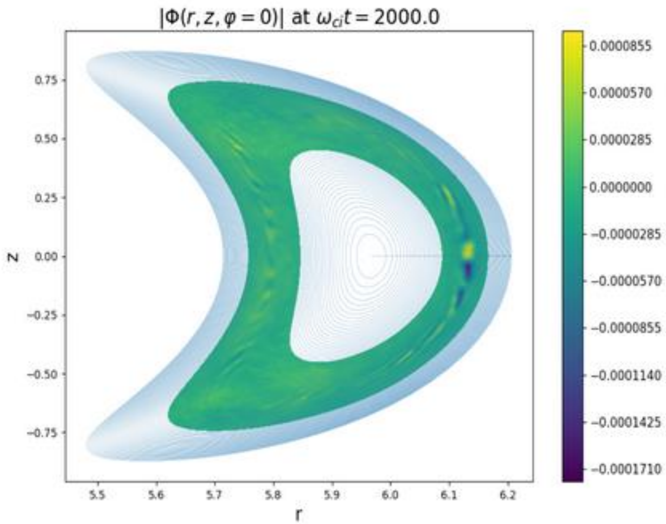

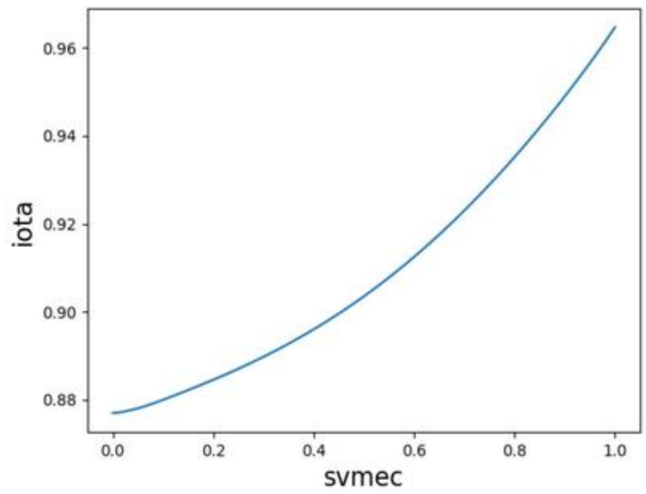

Larger temperature implies larger ρ_*

Larger ρ_* need less Fourier harmonics (to resolve the same $k\,\rho_i \sim 1$)

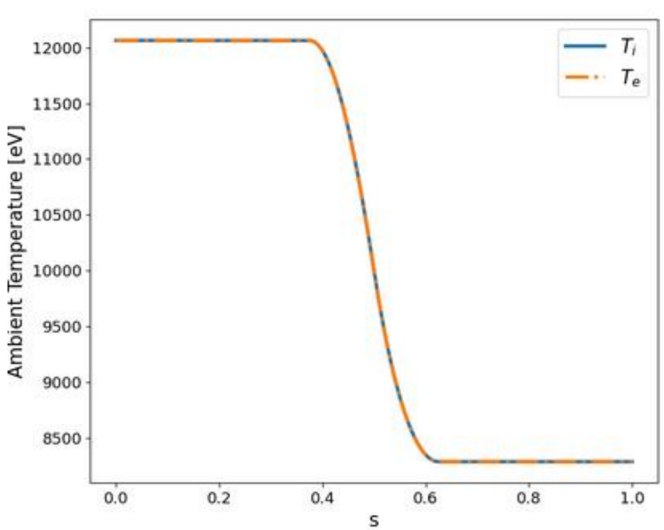

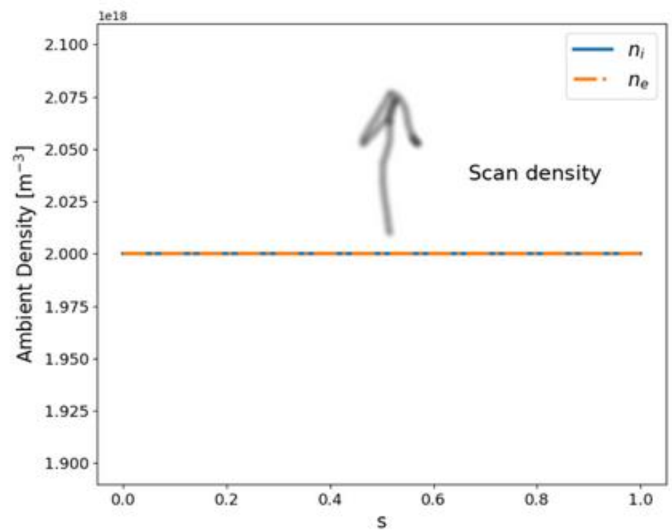

EM Euterpe simulations in W7-X (KJM)

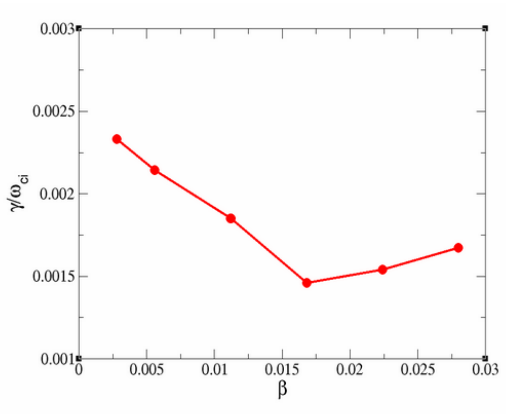

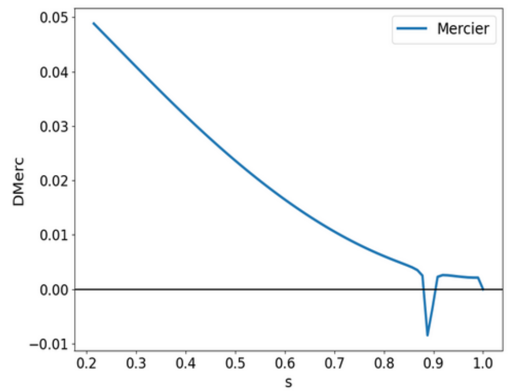

Mercier-stable W7-X
KBM transition observed
Mode saturation for KBM
No EM „run-away“
Zonal flows and microinstabilities coexist.

Mercier stability condition (see [Landerman, Jorge]):

$$D_{\mathrm{Merc}} = D_{\mathrm{Shear}} + D_{\mathrm{Curr}} + D_{\mathrm{Well}} + D_{\mathrm{Geod}} > 0$$

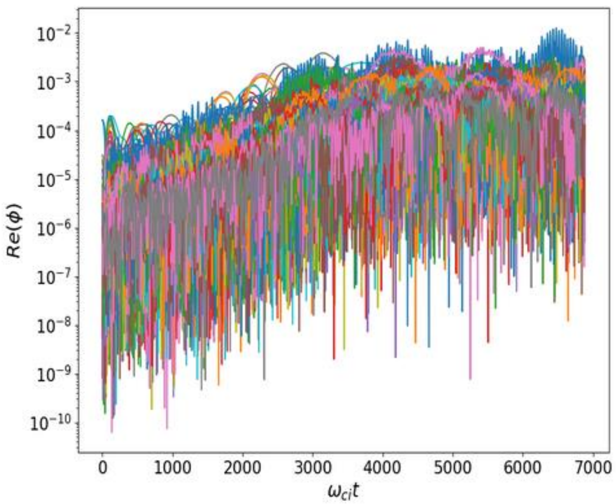

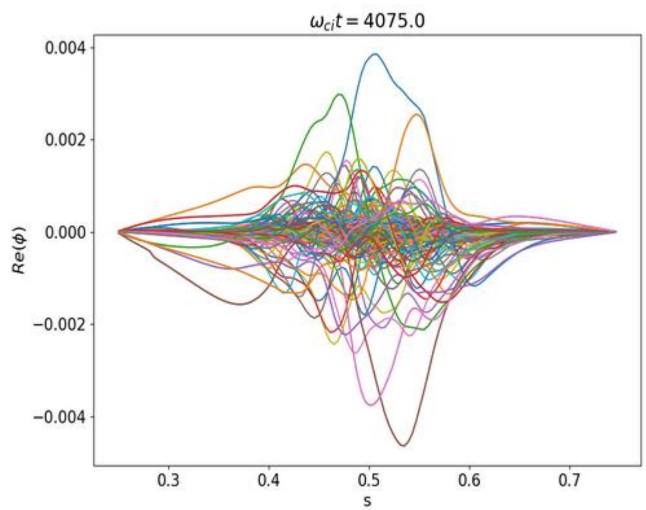

Saturation of the instability and the mode structure for $\beta = 2.8\%$

Toroidal spectrum: ZF and KBMs

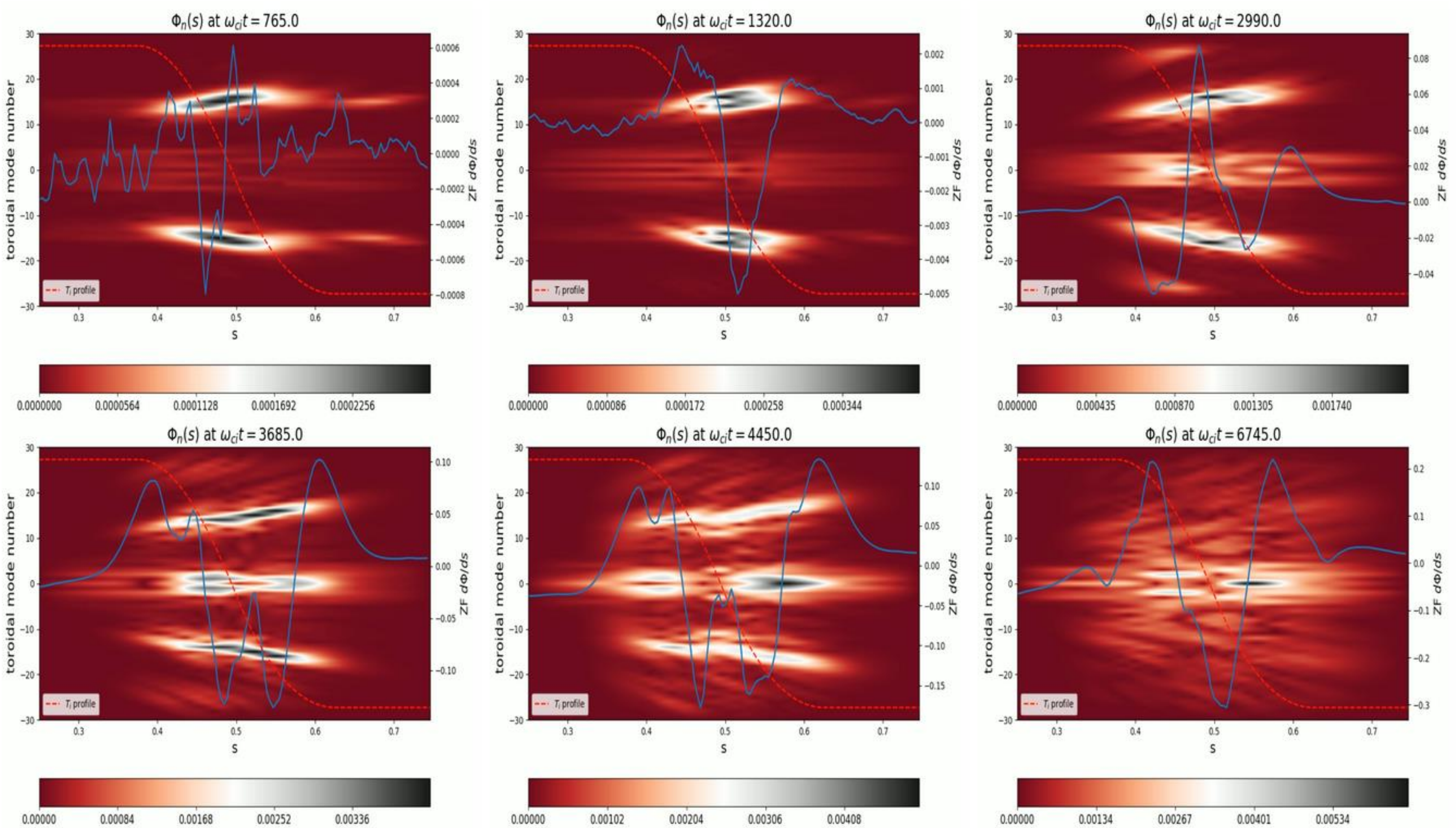

Toroidal spectrum and zonal flow evolution for $\beta = 2.8\%$

Zonal electric field (blue curve) driven self-consistently by stellarator turbulence

Plasma profile and radial fluxes: KBM in W7-X

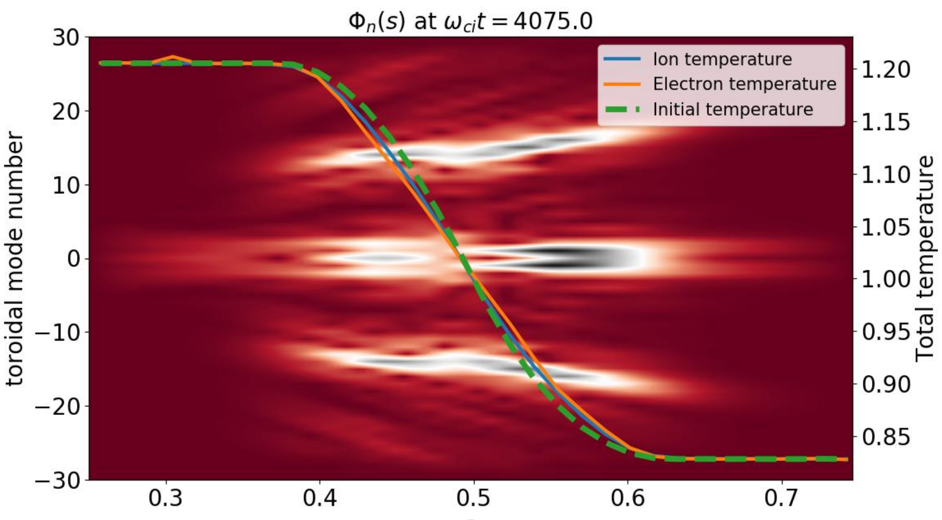

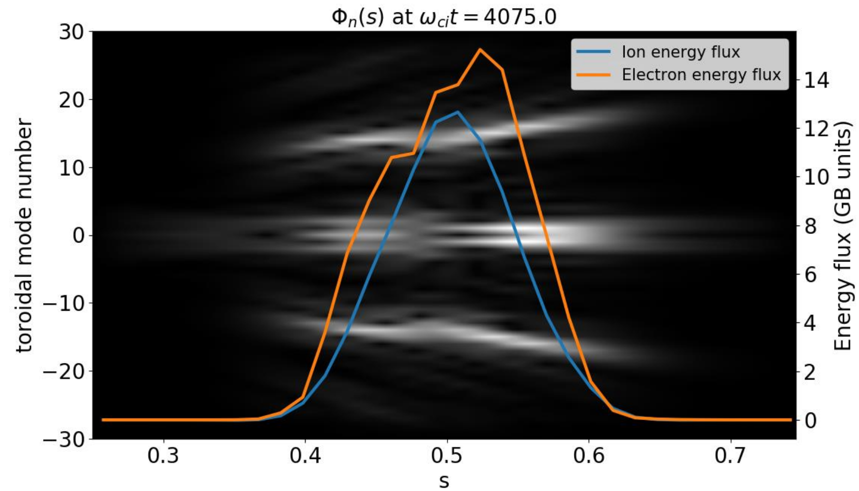

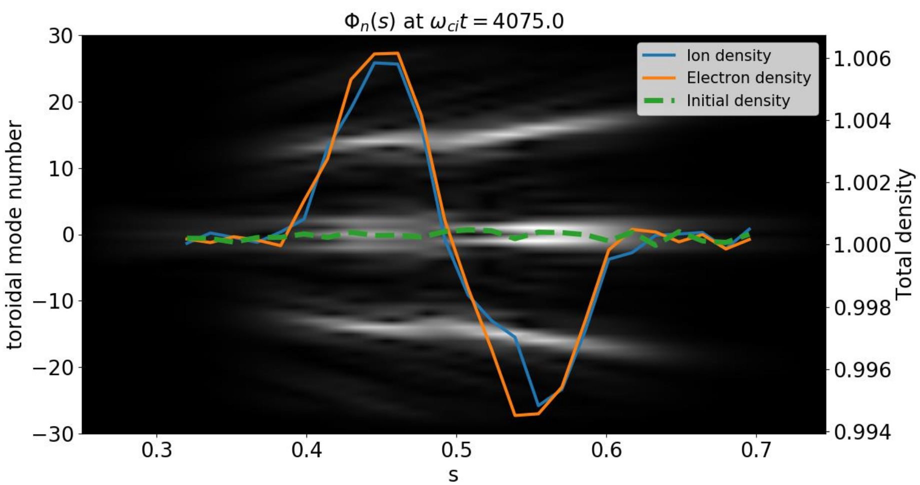

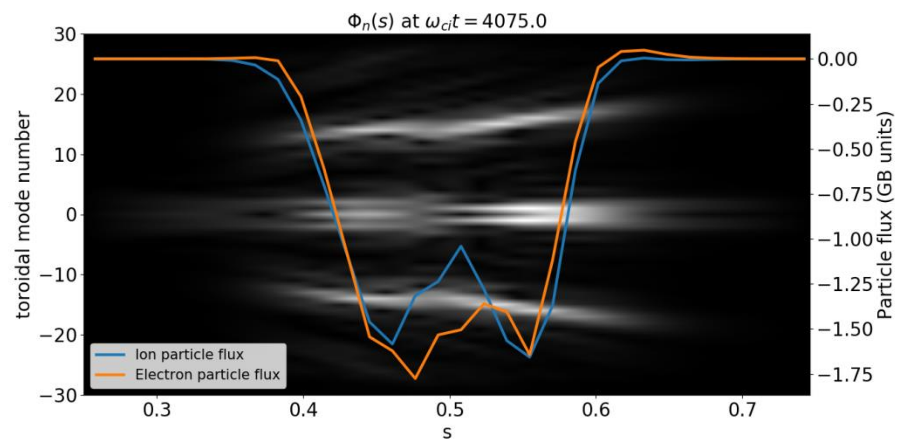

Inward particle flux

Simulations on MareNostrum

Four cases have been considered:

- hydrogen plasma in low-beta W7-X KJM configuration (ITG regime) and
- high-beta W7-X KJM configuration (KBM regime),
- D-T plasma in W7-X UFM configuration,
- H-Ar plasma in W7-X UFM configuration.

Main question was related to the particle transport.

- In H plasma, flat electron temperature profile: still inward particle flux (STELLA)?
- In D-T plasma, how does the turbulence transport different isotopes?
- In H-Ar plasma, how the turbulent impurity flux is directed?

Particle transport for flat Te

For flat electron temperature profile, the particle flux is indeed **outward**!
Also, the low-mode-number part of the spectrum is much weaker in this case.
Here, β=2.8% (KBM)

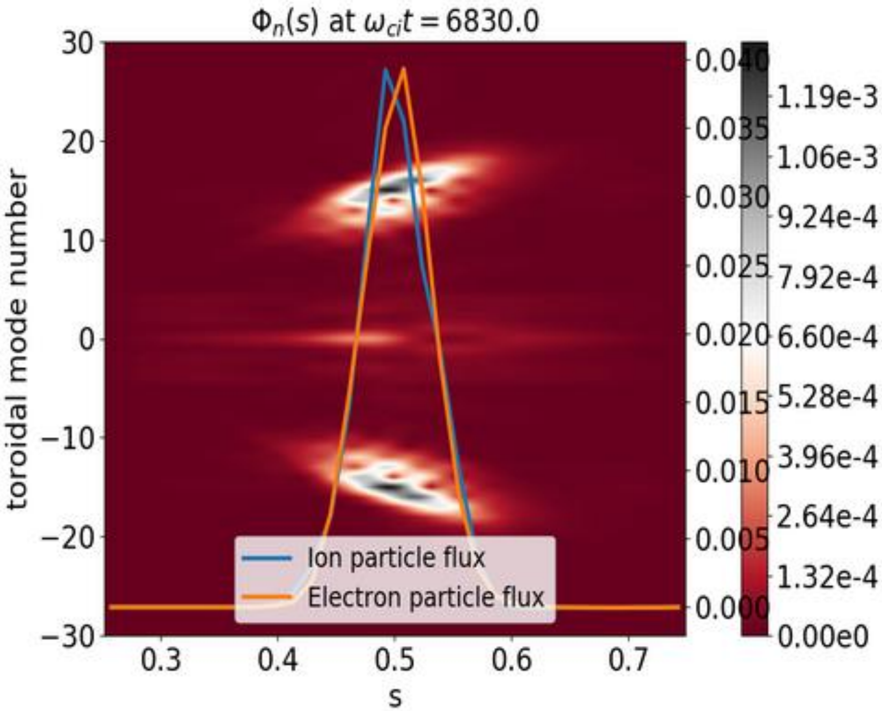

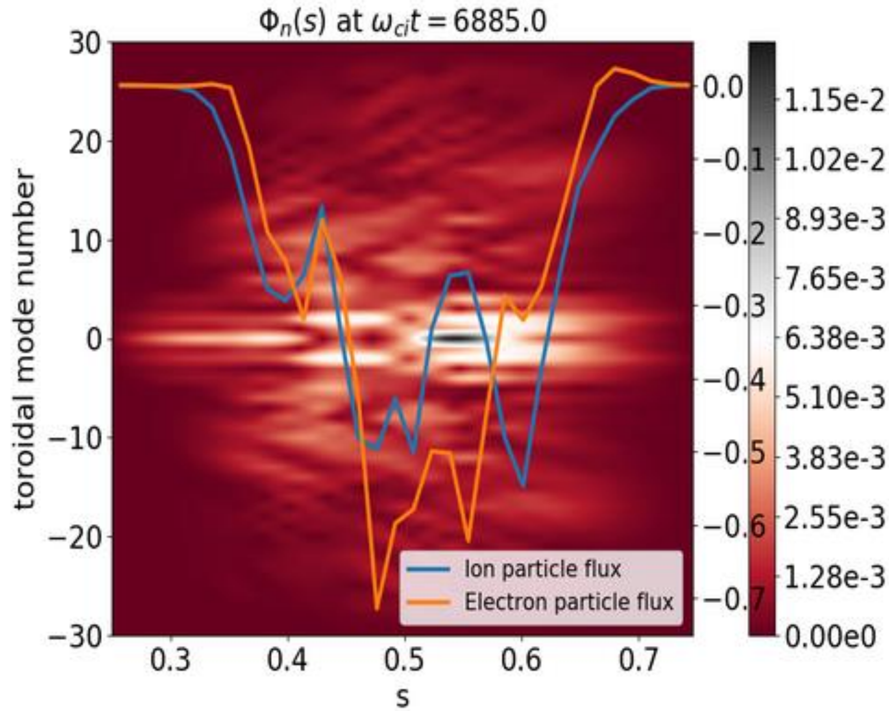

Left: flat electron temperature (dTe/dx = 0).
Right: same electron and ion temperature profiles (finite dTe/dx).
For β=0.28% (ITG) the trend is the same with low-n part of the spectrum better developed.

Heat and particle fluxes in H plasma

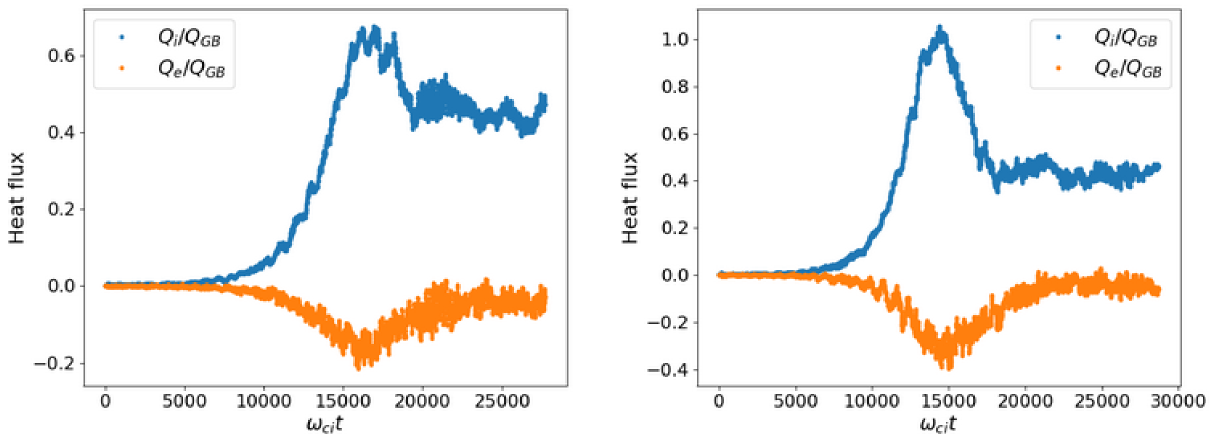

Left: low beta KJM (heat flux, H plasma). Right: high beta KJM (heat flux, H plasma)

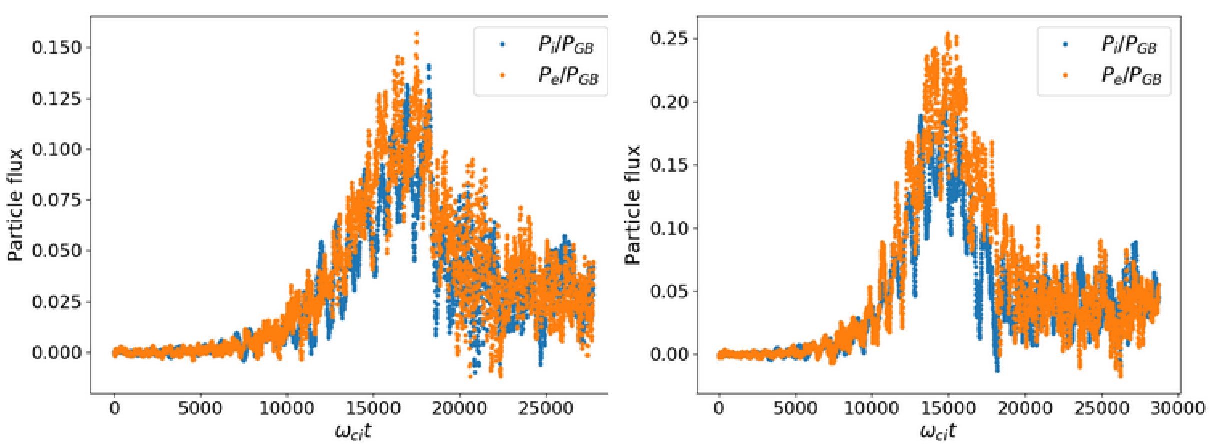

Outward particle flux
for flat electron profile!

Left: low beta KJM (particle flux, H plasma). Right: high beta KJM (particle flux, H plasma)

Particle transport in multi-ion plasmas

Particle flux is not the same for Deuterium and Tritium which may lead to isotope separation.
Opposite turbulent particle flux observed for impurities (Ar) and the main plasma (H).

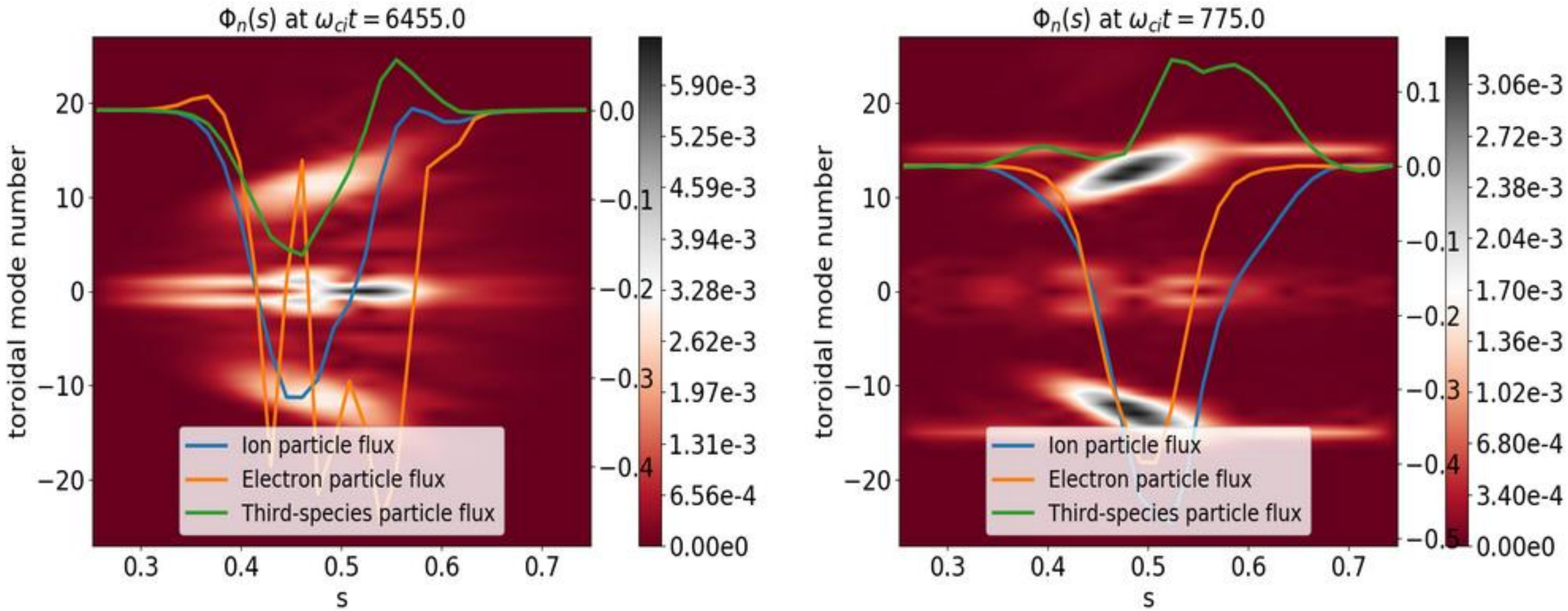

Turbulence may transport impurities outwards with inward bulk plasma particle flux!

Heat and particle transport in multi-ion plasmas

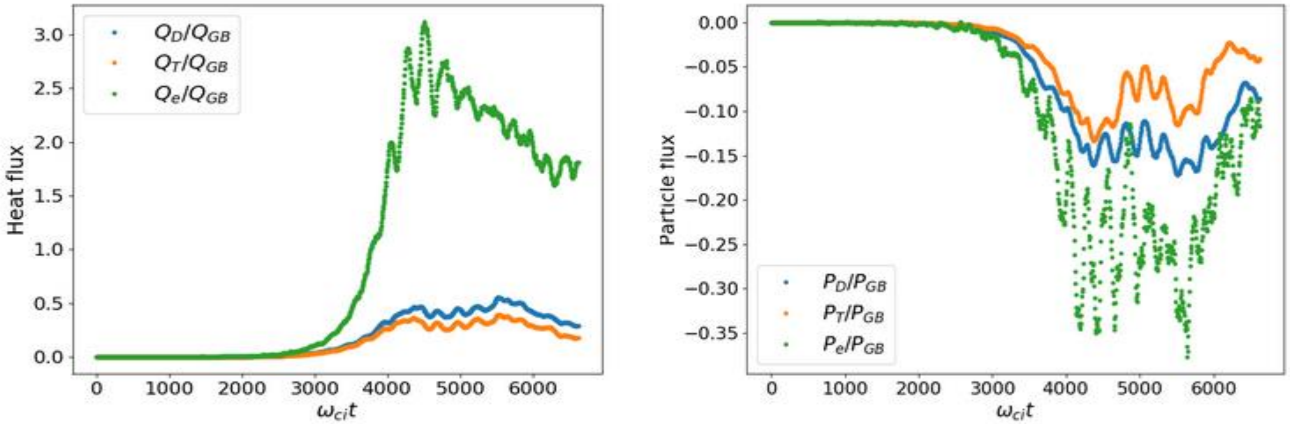

D and T are transported at different rates; Isotope separation by turbulence?(speculative)

Left: heat flux in DT plasma. Right: particle flux in DT plasma.

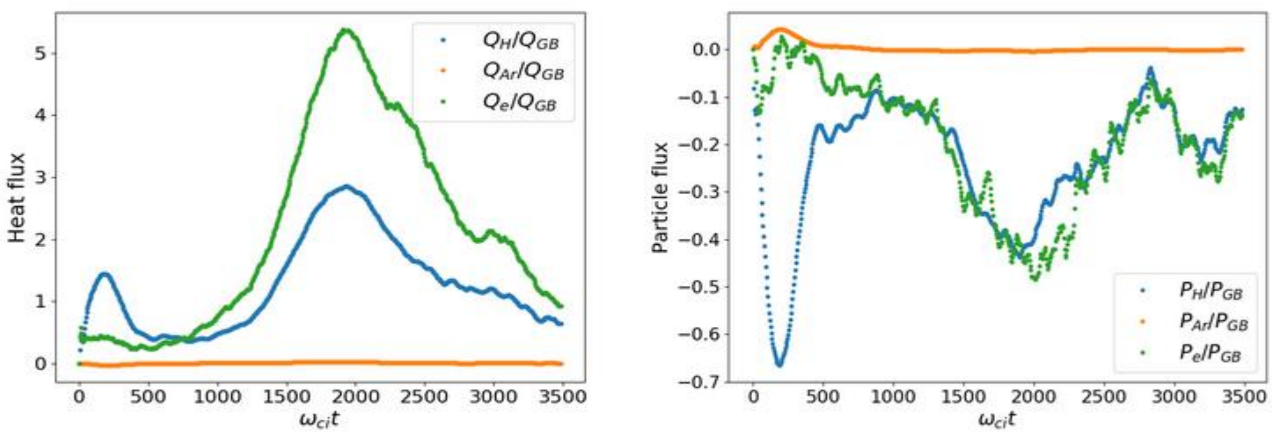

Two phases of evolution with Ar (speculative):

1) Ar flushed out
2) Turbulence is weak in presence of Ar
3) Stronger turbulence when Ar is gone

Left: heat flux in H-Ar plasma. Right: particle flux in H-Ar plasma.

Next steps on MareNostrum

1) Replacing Krook with markers' weight smoothing and employing heating sources in electromagnetic simulations will be explored.

2) Profiles with radially delocalized instability sources will be considered (EM turbulence).

3) Transition from ITG/TEM to KBM will be addressed **on GPUs** in linear global EM simulations (configurations of W7-X, LHD, and TJ-II; new optimized configurations).

4) Simulations of linear zonal flow (ZF) dynamics in EM simulations will be addressed in selected configurations of W7-X. Results will be compared to those obtained with electrostatic simulations. These simulations will allow testing the performance of the formulas used in [SanchezPPCF18]. **Attempt GPUs** for these runs.

5) Effect of multi-ions on linear EM stability (ITG/TEM-KBM transition) and ZF oscillations. **Attempt GPUs** for these runs.

Effect of β and $\delta B_{||}$ in W7-X (KJM)

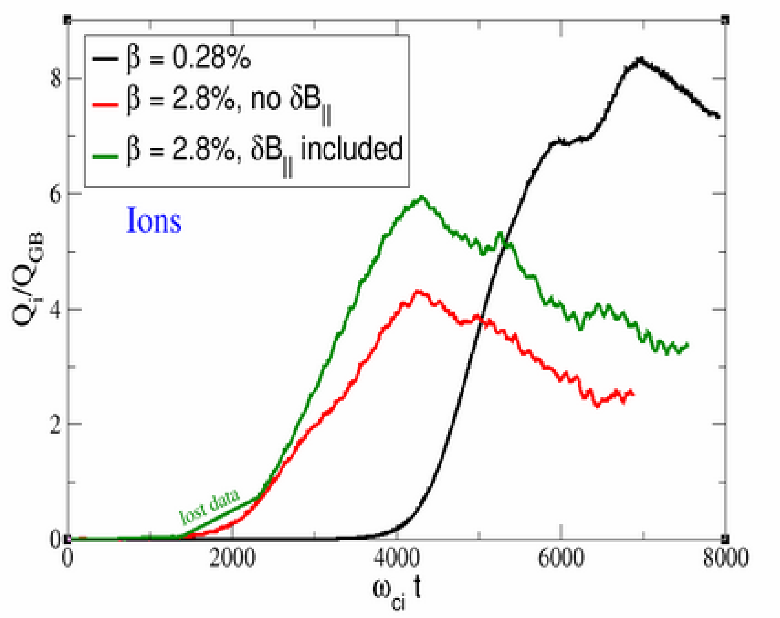

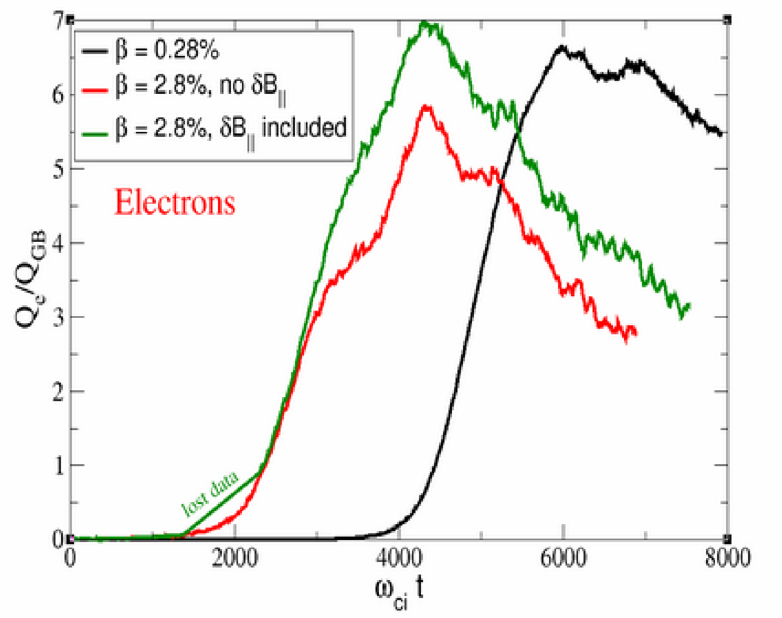

Effect of β (decreasing the heat flux) and $\delta B_{||}$ (increasing the heat flux). The electron heat flux at large β and including $\delta B_{||}$ exceeds the electron heat flux at small β

Suggests that:

1) finite beta reduces turbulence
2) this happens only when $\delta B_{||}$ is neglected
3) consistent equilibrium is important

Model for $\delta B_{||}$ in EUTERPE

Equations of motion solved by EUTERPE (note that μ is the magnetic moment per mass):

$$\dot{\vec{R}} = (v_{\|} - \frac{q}{m}\langle A_{\|}\rangle)\vec{b}^{*} + \frac{1}{B_{\|}^{*}}\vec{b} \times \left(\frac{m}{q}\mu\nabla B + \nabla\langle\Psi\rangle + \frac{m}{q}\mu\,\nabla\delta B_{\|}\right)$$

$$\dot{v}_{\|} = -\frac{q}{m}\vec{b}^{*}\left(\frac{m}{q}\mu\nabla B + \nabla\langle\Psi\rangle + \frac{m}{q}\mu\nabla\delta B_{\|}\right)$$

<<…>> = (…) (disk-average)

<…> = (…) (gyro-average)

closed by the pressure balance: $\mu_0\nabla_{\perp}\delta p_{\perp} + B\nabla_{\perp}\delta B_{\|} = 0$

$$\delta B_{\|} = -\frac{\mu_0}{B}\sum_{s=i,e} m_s \int \mu B\delta f_s \delta(\vec{R} - \vec{x})\mathrm{d}^6 z$$

Quasineutrality equations and parallel Ampere's law are not modified. Definitions:

$$\mu = \frac{v_{\perp}^2}{2B}, \quad \vec{B}^{*} = \vec{B} + \frac{m}{q}v_{\|}\nabla\times\vec{b}$$

$$\mathrm{d}^6 z = B_{\|}^{*}\,\mathrm{d}^3 R\,\mathrm{d}v_{\|}\,\mathrm{d}\mu\,\mathrm{d}\alpha, \quad \Psi = \Phi - v_{\|}A_{\|}, \quad \langle\Phi\rangle = \frac{1}{2\pi}\int\Phi(\vec{R}+\vec{\rho})\mathrm{d}\alpha$$

Exact formulation would require the replacement: $\mu\delta B_{||}(\vec{R}) \Longrightarrow \mu \ll \delta B_{||} \gg$

Here, $\ll \delta B_{||} \gg = \frac{1}{\pi\rho^2}\int \delta B_{||}\,(\boldsymbol{R}+\boldsymbol{\rho})\,\mathrm{d}\Sigma$ is the disk average with $\mathrm{d}\Sigma = \rho\,\mathrm{d}\rho\,\mathrm{d}\theta$

ITG-optimized stellarators (“W7-K“ configuration)

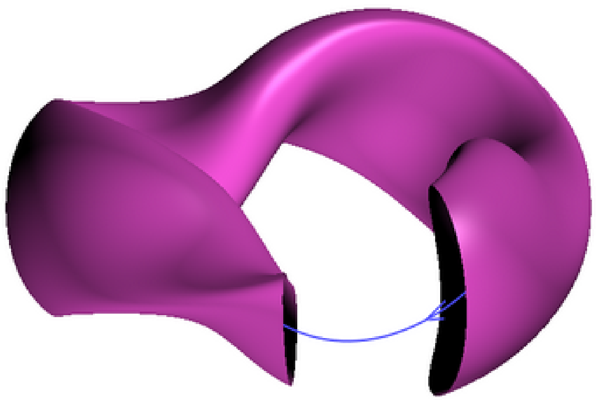

About configuration

Rmajor, R: 1.9833
rminor, a: 0.49442
Volume: -9.5698
2pi^2*R*a^2: 9.5698
# of periods: 3
# of pol.mods, M: 11
# of tor.mods, N: 12
# of flux.surfs: 159

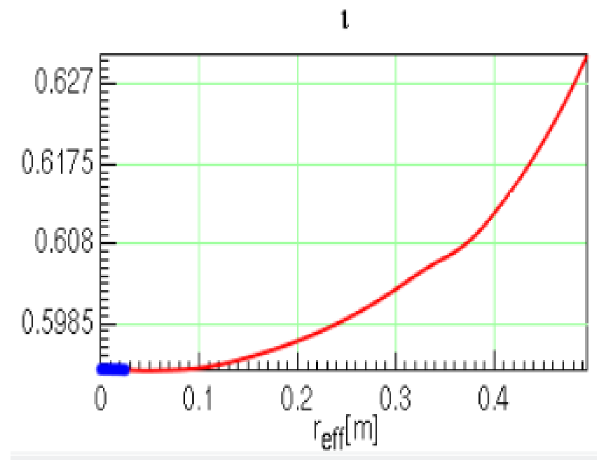

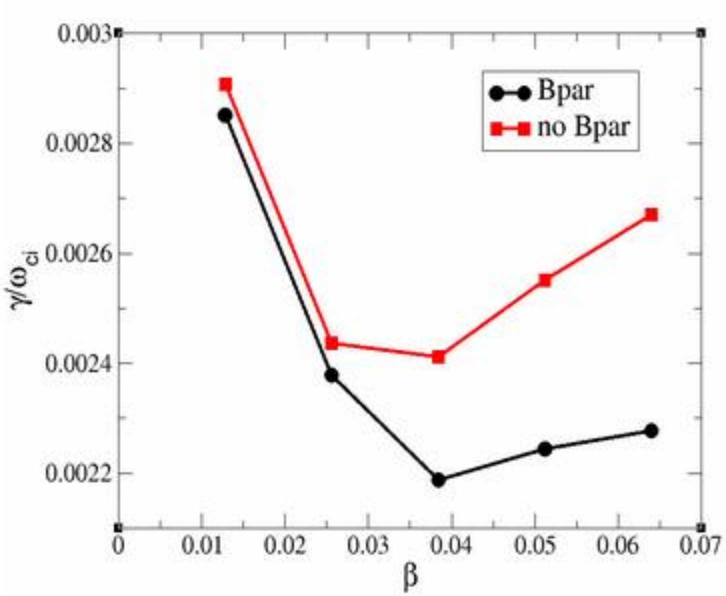

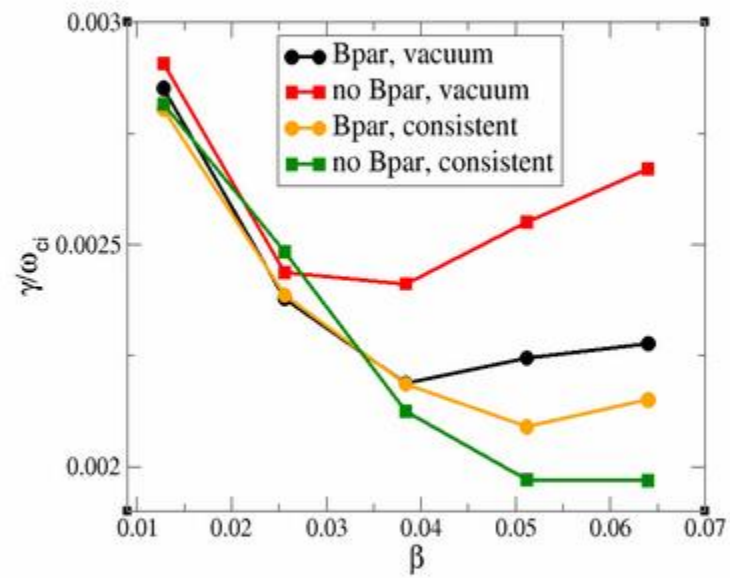

Choice of self-consistent equilibrium affects the result

EM Simulations in W7-K

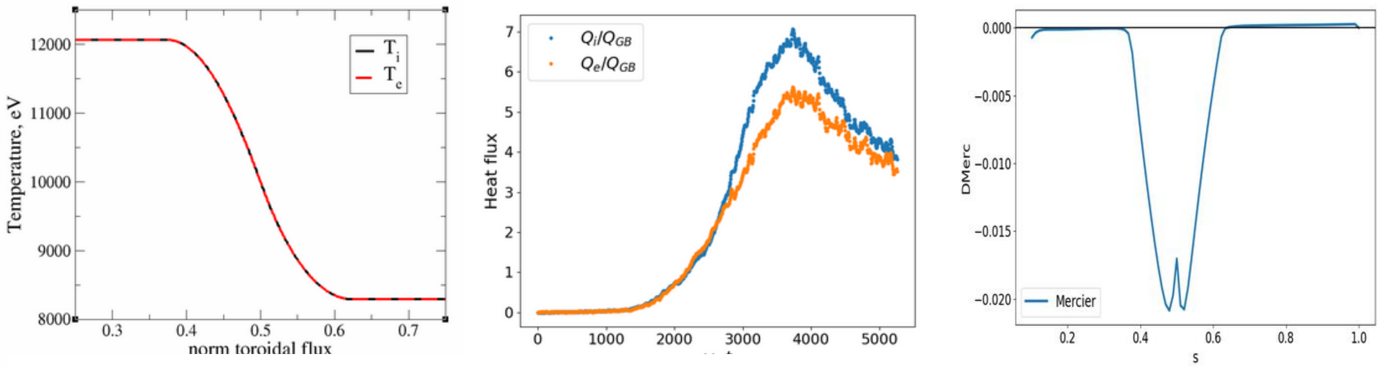

Mercier-unstable geometry

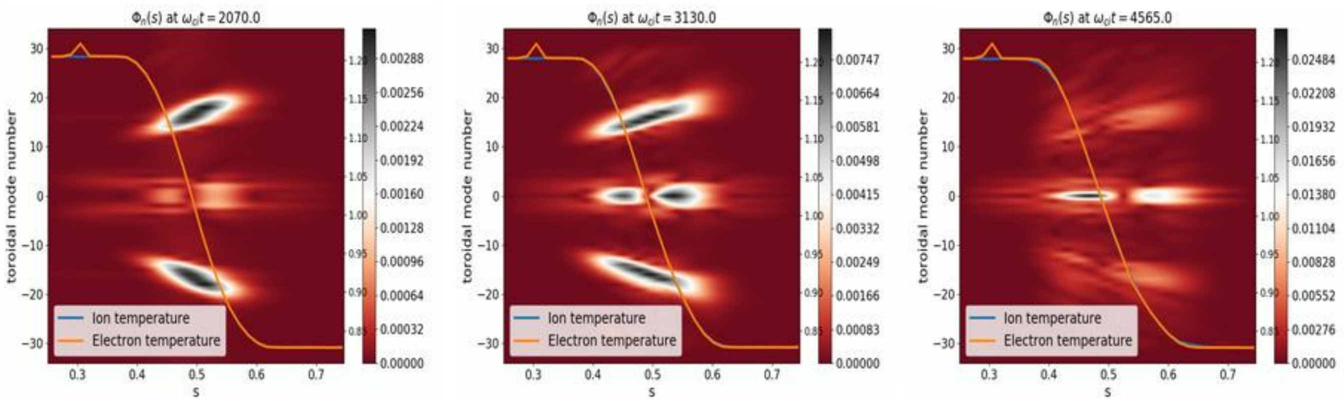

Turbulent spectral evolution

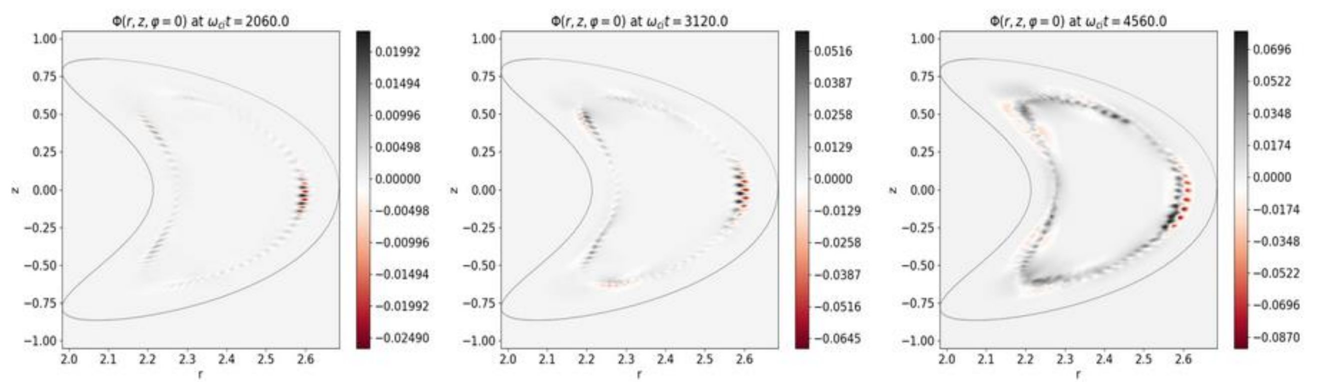

Evolution in real space

„Realistic-size“ W7-X („UFM“ configuration)

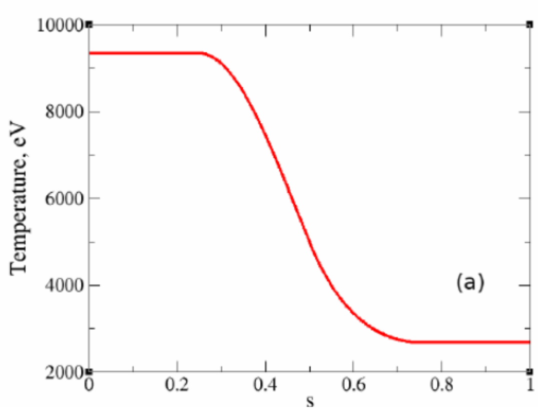

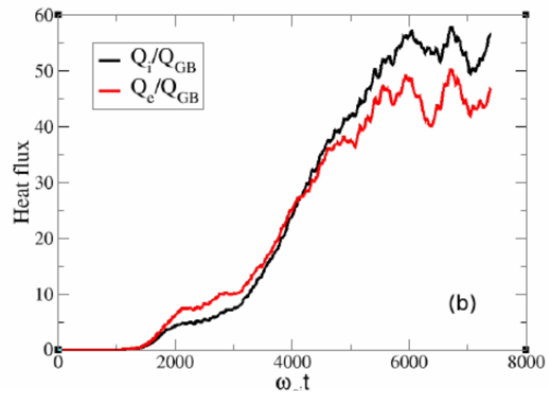

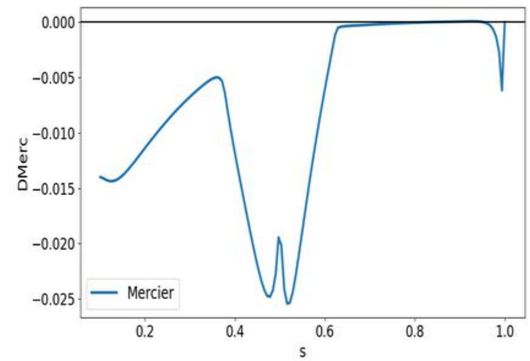

Mercier unstable

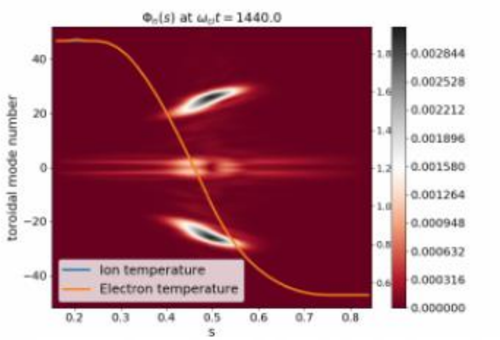

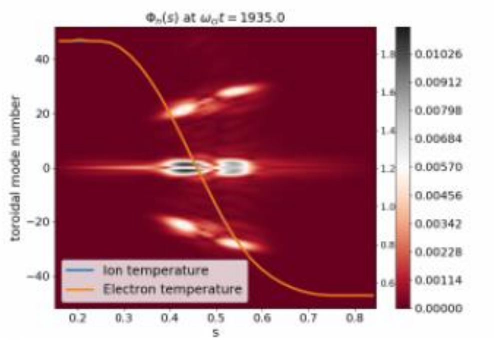

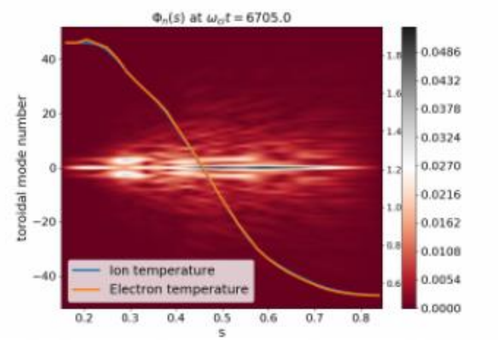

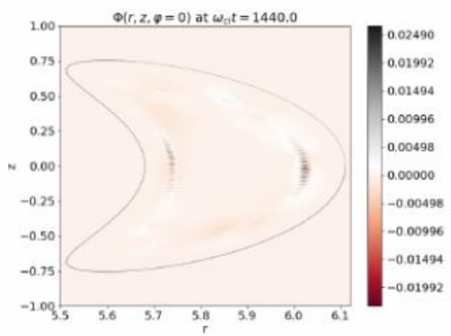

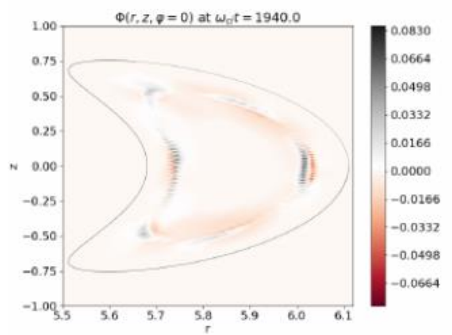

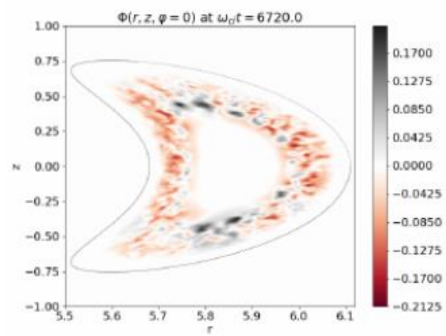

Computationally very challenging

Summary

- Electromagnetic turbulence plays an important role in stellarators.
- In the past, most nonlinear gyrokinetic simulations were performed in a flux tube.
- Here, global electromagnetic turbulence is simulated in stellarator geometry using the gyrokinetic particle-in-cell code EUTERPE.
- Evolution of the turbulent electromagnetic field and the plasma profiles is computed at different plasma beta and for different magnetic configurations of W7-X and W7-K.
- Turbulence is linearly driven at high toroidal mode numbers. Nonlinearly, lower toroidal mode numbers, including zonal flows, are excited.
- Parallel magnetic field and equilibrium affect the result.

BACK-UP

Simulations in down-scaled W7-X

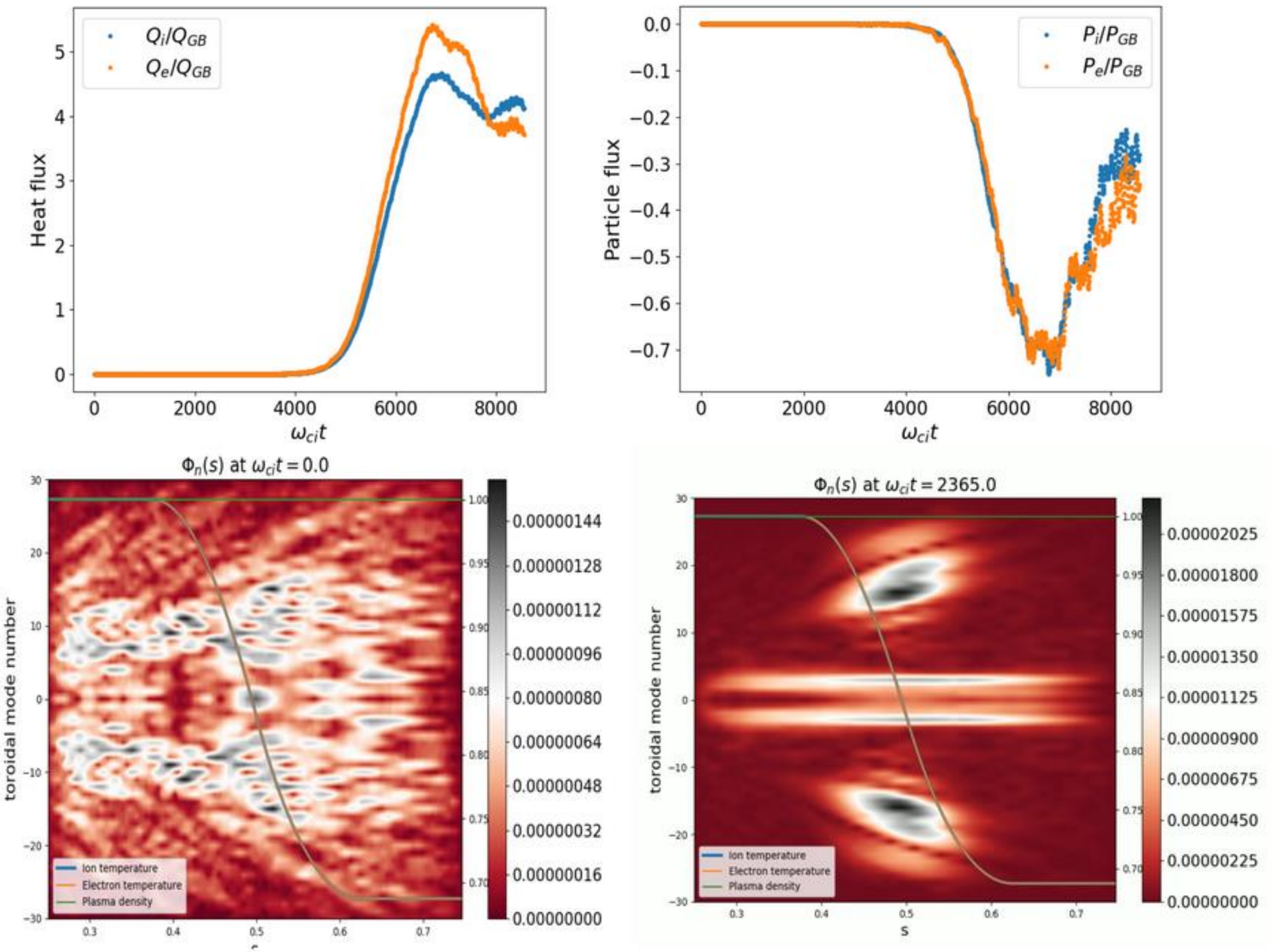

Initialization with noise; instability starts to develop

Simulations in down-scaled W7-X

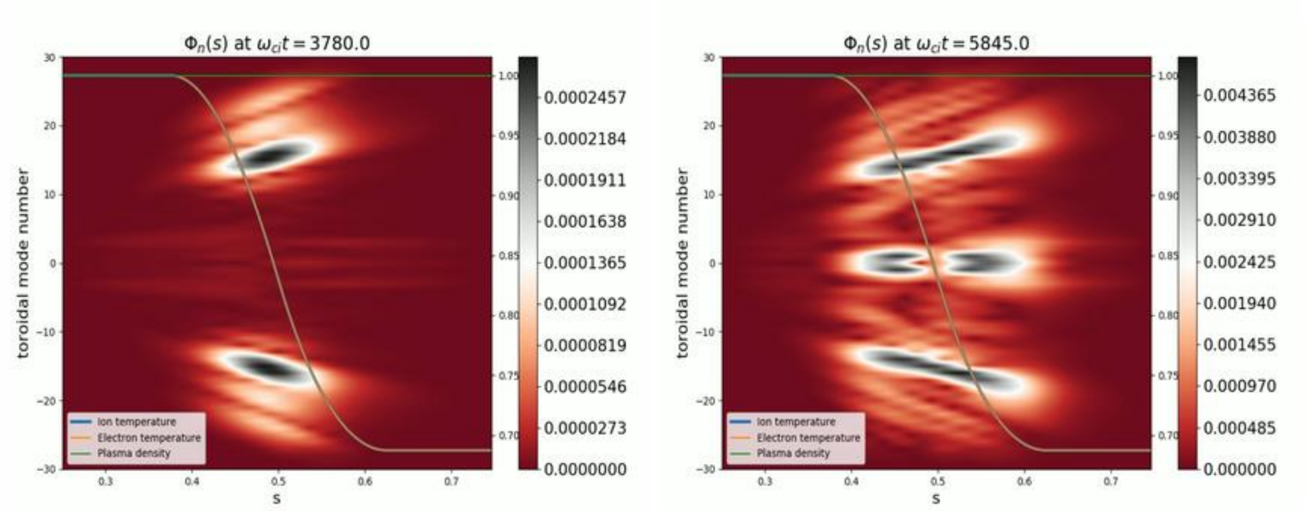

Linear instability; ZF is excited; linear mode is weaken locally by ZF

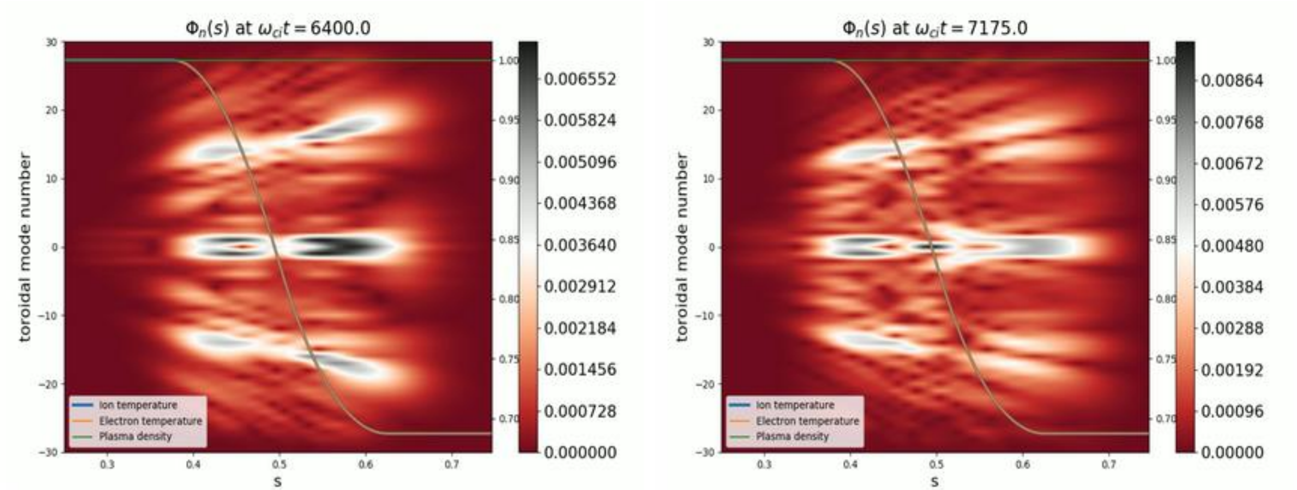

The turbulence is pushed by ZF into regions of small gradient; saturation